

Accuracy of first-principles interatomic interactions and predictions of ferroelectric phase transitions in perovskite oxides: Energy functional and effective Hamiltonian

Arpita Paul,¹ Jianwei Sun,² John P. Perdew,^{3,4} and Umesh V. Waghmare^{1,*}

¹*Theoretical Sciences Unit, Jawaharlal Nehru Centre for Advanced Scientific Research, Jakkur, Bangalore 560 064, India*

²*Department of Physics, The University of Texas at El Paso, El Paso, Texas 79968, USA*

³*Department of Physics, Temple University, 1925 North 12th Street, Philadelphia, Pennsylvania 19122, USA*

⁴*Department of Chemistry, Temple University, 1901 North 13th Street, Philadelphia, Pennsylvania 19122, USA*

(Received 22 November 2016; published 15 February 2017)

While first-principles density functional theory (DFT)-based models have been effective in capturing the physics of ferroelectric phase transitions in BaTiO₃, PbTiO₃, and KNbO₃, quantitative estimates of the transition temperatures (T_C) suffer from errors that are believed to originate from the errors in estimating lattice constants obtained within the local density approximation (LDA) and generalized gradient approximation (GGA) of DFT. The recently developed strongly constrained and appropriately normed (SCAN) meta-GGA functional has been shown to be quite accurate in the estimation of lattice constants. Here, we present a quantitative analysis of the estimates of ferroelectric ground-state properties of eight perovskite oxides and transition temperatures of BaTiO₃, PbTiO₃, and KNbO₃ obtained with molecular dynamics simulations using an effective Hamiltonian derived from the SCAN meta-GGA-based DFT. Relative to LDA, we find an improvement in the estimates of T_C , which arises from the changes in the calculated strain-phonon, anharmonic coupling constants, and strength of ferroelectric instabilities, i.e., frequencies of the soft modes. We also assess the errors in T_C originating from approximately integrating out the high-energy phonons during construction of the model Hamiltonian through estimates of the effects of fourth-order couplings between the soft mode and higher-energy modes of BaTiO₃, PbTiO₃, and KNbO₃. We find that inclusion of these anharmonic couplings results in deeper double-well energy functions of ferroelectric distortions and further improvement in the estimates of transition temperatures. Consistently improved estimates of lattice constants and transition temperatures with the SCAN meta-GGA calculations augur well for their use in simulations of superlattices or heterostructures of perovskite oxides, in which the effects of lattice matching are critical.

DOI: [10.1103/PhysRevB.95.054111](https://doi.org/10.1103/PhysRevB.95.054111)

I. INTRODUCTION

Ferroelectrics are an important class of materials that exhibit a spontaneous macroscopic electric polarization that is switchable with application of an electric field, and hence have a wide range of technological applications [1,2]. Perovskite oxides are the most interesting of ferroelectric materials and have been studied frequently [3,4] since the discovery of barium titanate in 1945 [5]. Perovskite oxides have a chemical formula ABO₃, with the A cation at the corner of the cube, and with the B and O atoms located at the body-centered and face-centered positions, respectively. There is a remarkable diversity in the structural instabilities and phase transitions that these perovskites undergo: ferroelectric transitions (associated with polar distortion) in BaTiO₃, PbTiO₃, and KNbO₃, antiferroelectric transition (involving nonpolar distortion) in PbZrO₃, and antiferrodistortive transition (associated with tilting of oxygen octahedra) in SrTiO₃ [4,6]. These phase transitions and competing instabilities have singularly important consequences to their properties relevant to technological applications. First-principles density functional theoretical (DFT) calculations have been used extensively in microscopic studies of structural transitions via identifying the responsible phonon mode for structural transition, studying the stability of the intermediate phases, and predicting transition temperatures (T_C) [4,7–9]. It has been established that harmonic and

anharmonic couplings between phonons and strain-phonon coupling constants are the most crucial parameters that govern the phase transitions in perovskites [4,8,10]. Accuracy in the determination of these parameters and subsequent estimation of transition temperatures is naturally limited by the DFT errors in the estimation of lattice constants.

Earlier all-electron calculations using the full potential linearized augmented plane-wave (FLAPW) method within local density approximation (LDA) predicted the cubic phases of KNbO₃ to be stable (in contradiction to experimental results), and PbTiO₃ and BaTiO₃ to be unstable at the optimized lattice constant [4,11]. The discrepancies between experimental and theoretical results (using LDA) for cubic KNbO₃ have been removed by implementing ultrasoft pseudopotentials [4]. But, LDA is well known to underestimate the lattice constant by 1–2% as it neglects the effects of inhomogeneity in electron density [4,12]. Such overbinding of the structure predicted within LDA results in underestimation of the difference in energies of cubic and distorted structures [13]. This is because the ferroelectric instability is a strong function of cell volume of those materials [13,14].

While *ab initio* molecular dynamics (MD) or Monte Carlo (MC) simulations would be effective in the estimation of the temperature-dependent transition properties, the size (length scale) of a system needed to capture the phase transition and corresponding computational cost make them presently impractical. Instead, an approximate approach is adopted that uses an effective Hamiltonian, which focuses on the low-energy structural configurations in MD or MC simulations

*waghmare@jncasr.ac.in

[7,8]. Thus, there are two sources of errors in the first-principles description of ferroelectric transitions: (a) those arising from the choice of DFT functional and (b) those arising from the truncation of the set of configurations through the effective Hamiltonian.

As an example, the too-shallow potential well in BaTiO₃ underestimates the transition temperature (T_C) determined using a parametrized effective Hamiltonian based on LDA [7]. However, this problem was resolved by applying a negative pressure to the system [7]. Also, the value of T_C of PbTiO₃ using interaction parameters (calculated using LDA) at the experimental lattice constant is underestimated [8]. On the other hand, the generalized gradient approximation (GGA) mostly overestimates the lattice constants and gives supertetragonal structures of PbTiO₃ and BaTiO₃ [14]. By including the density gradient, GGAs can predict accurate structures or energies, but not both together [15,16]. This suggests an important avenue for further functional development which can correctly capture structural properties, i.e., lattice constant, anharmonic coupling between phonon modes, and strain-phonon coupling parameters, which are relevant to the structural transition. The GGA functional proposed by Wu and Cohen (WC-GGA) has been known to accurately calculate the ferroelectric properties of BaTiO₃ and PbTiO₃ [17]. However, the WC-GGA fails to precisely determine the properties of atoms and molecules, as it was constructed for solids (slowly varying electron density) [17].

The recently developed nonempirical strongly constrained and appropriately normed semilocal density functional (SCAN) has been shown to estimate accurate structures and energetics of diversely bonded molecules and materials (for slowly as well as rapidly varying electron densities) and to improve the band gap, which was underestimated by LDA and GGA [18–21]. The SCAN meta-GGA satisfies all of the 17 known exact constraints (about 6 for exchange, 6 for correlation, and 5 for the sum of the two) appropriate to semilocal functionals by including the orbital kinetic energy densities [18]. The calculations are computationally more expensive using SCAN meta-GGA than normal GGA or LDA, but SCAN is more efficient than hybrid functionals due to its semilocal nature.

Here, we present the ground-state properties of eight perovskites, i.e., BaTiO₃, CaTiO₃, SrTiO₃, PbTiO₃, KNbO₃, NaNbO₃, PbZrO₃, and BaZrO₃, using the SCAN meta-GGA functional and notice a significant improvement of lattice constants and band gaps of eight oxides compared to earlier theoretical results using LDA [4]. We then estimate T_C of BaTiO₃, PbTiO₃, and KNbO₃ using the parametrized effective Hamiltonian based on the SCAN meta-GGA functional, calculate the lowest-order coupling between soft mode and higher-energy modes, and determine the consequences of approximations in construction of the effective Hamiltonian for finite-temperature properties.

II. METHODS

First-principles calculations based on density functional theory have been performed here on eight perovskites using the SCAN meta-GGA exchange-correlation functional as implemented in the VASP code [18,22,23]. For calculations, we

use projector augmented wave (PAW) potentials containing a contribution from kinetic energy density of the core electrons [24]. We have considered eight oxides, i.e., BaTiO₃, SrTiO₃, PbTiO₃, CaTiO₃, KNbO₃, NaNbO₃, PbZrO₃, and BaZrO₃, for determining ground-state properties. We use 5s and 5p states of Ba, 3s state (3s and 3p states) of K (Ca), 4s and 4p states of Sr, Zr, and Nb, 2p state of Na, and 5d state of Pb as valence states. An energy cutoff of 560 eV has been used to truncate the plane-wave basis used to represent wave functions. Integrations over the Brillouin zone were sampled on an $8 \times 8 \times 8$ uniform mesh of k points.

MD simulations for studying the phase transitions of BaTiO₃, PbTiO₃, and KNbO₃ (considering the effective Hamiltonian from Ref. [7]) are performed using the FERAM code [7,25,26]. At each temperature in our simulation within the canonical ensemble, temperature is kept fixed using the Nosé-Poincaré thermostat [27]. The time step was set to $\Delta t = 2$ fs. We use a supercell of system size $L_x \times L_y \times L_z = 16 \times 16 \times 16$ and temperature step ± 5 K in heating-up and cooling-down simulations. We use 20 000 thermalization steps and 40 000 steps for averaging properties of the system at each temperature. The initial configuration used in cooling-down simulations of all three compounds is a paraelectric state with $\langle u_\alpha \rangle = 0.0$ ($\alpha = x, y, z$) and $\langle u_\alpha^2 \rangle - \langle u_\alpha \rangle^2 = (0.12 \text{ \AA})^2$. In the heating-up simulation, we choose ferroelectric states of three compounds ($\langle u_z \rangle = 0.33 \text{ \AA}$ and $\langle u_x \rangle = \langle u_y \rangle = 0.0$ for PbTiO₃, and $\langle u_\alpha \rangle = 0.11 \text{ \AA}$ for BaTiO₃ and KNbO₃) as initial configurations.

III. RESULTS AND DISCUSSION

A. Ground-state properties

1. Structural and electronic properties

We optimized the lattice parameters of the cubic perovskite structures of eight ABO₃ compounds, i.e., BaTiO₃, SrTiO₃, CaTiO₃, PbTiO₃, KNbO₃, NaNbO₃, PbZrO₃, and BaZrO₃, using the SCAN meta-GGA functional. Our results in comparison with LDA are shown in Fig. 1 [4]. The lattice constants of cubic SrTiO₃, CaTiO₃, PbZrO₃, and BaZrO₃ are overestimated slightly by 0.1–0.5% (see Fig. 1), whereas for other compounds, lattice constants are underestimated at the most by 0.8% relative to the experimental values [4]. Lattice constants optimized using SCAN are better compared to the earlier theoretical results obtained from calculations considering all-electron (FLAPW) and ultrasoft pseudopotentials with LDA [4]. Lattice parameters of cubic BaTiO₃, PbTiO₃, and SrTiO₃ are overestimated by 0.2% from the values obtained using the WC-GGA functional [7].

We then optimized lattice constants of the tetragonal phases of BaTiO₃ and PbTiO₃ (as shown in Table I). The SCAN-based calculated values of a of tetragonal phases of BaTiO₃ and PbTiO₃ are within 0.025% of experimental values and are better than earlier theoretical results using LDA, Perdew-Burke-Ernzerhof (PBE)-GGA, and hybrid functionals [14]. The generalized gradient approximation (GGA) in the PBE parametrized form overestimates lattice constants and gives supertetragonal structures of BaTiO₃ and PbTiO₃ (see Table I). In addition, the differences in the z components of atomic positions between cubic and tetragonal phases of BaTiO₃

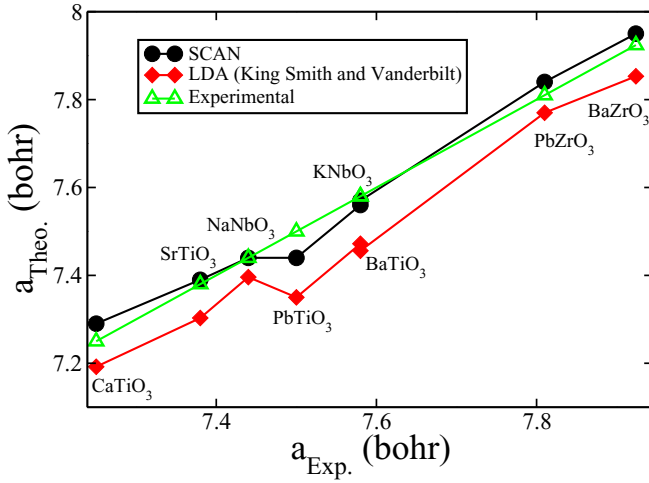


FIG. 1. Optimized lattice constants of eight cubic oxides using the SCAN meta-GGA functional in comparison with experimental and earlier theoretical (using LDA) lattice parameters [4]. Lattice constants (experimental and SCAN meta-GGA) of cubic KNbO₃ and BaTiO₃ are close to each other.

(ferroelectric distortion) are slightly overestimated compared to experimental values and are better than earlier theoretical results using LDA, PBE-GGA, and hybrid functionals [14]. For PbTiO₃, the level of agreement between experiment and our estimates of these differences in atomic positions is not that good. This overestimation of atomic displacements is caused by the slight overestimation of c/a ratios of PbTiO₃ (see Table I). We analyzed this in depth and found that the energy surface of PbTiO₃ is very flat (shallow) and small energy differences result in large changes in structural parameters. However, our estimates of c/a ratios of tetragonal BaTiO₃ and PbTiO₃ are better than those of other functionals (LDA, PBE-GGA, and hybrid) [14]. Our results for BaTiO₃ and PbTiO₃ are comparable to the earlier results obtained using the WC-GGA functional and treating Ti and O atoms at the all-electron level with Hartree-Fock (HF) pseudopotentials for Pb and Ba [14]. For KNbO₃, the c/a ratio (1.034) is slightly overestimated with SCAN compared to the experimental value (1.017) [28]. In addition, we optimized lattice parameters of orthorhombic

(a , b , and c) and rhombohedral (a and α) structures of BaTiO₃ and KNbO₃ using the SCAN meta-GGA functional (see Table II). Our SCAN meta-GGA-based estimates of lattice parameters of orthorhombic and rhombohedral phases are within 0.4% of experimental values [29–31]. The agreement with experiment is much better than that obtained with PBE-GGA and WC-GGA functionals [32].

Elastic constants of cubic perovskites have been determined from the stress-strain relationship. The elastic constants of BaTiO₃ using SCAN are comparable to the value obtained using LDA (see Table III). The values of the bulk modulus of KNbO₃ and PbTiO₃ are 197 and 203 GPa, respectively, which agree to about 2% with the values obtained earlier using LDA [4]. For SrTiO₃, elastic constants are within 16% of the experimental values [33]. It has been observed experimentally that C_{11} , C_{12} , and C_{44} of SrTiO₃ are strong functions of temperature, and decrease by 4% when the temperature drops from 30 °C to −160 °C [34]. The dependence of elastic constant on temperature has also been noticed experimentally for BaTiO₃ and PbTiO₃ [35]. As first-principles-based DFT calculations do not include the effect of temperature, we consider this deviation of elastic constants from the experimental values as acceptable. The exchange-correlation functional influences mostly C_{11} and C_{12} parameters for all materials. SCAN-based estimates of C_{11} are overestimated compared to experimental values, whereas other elastic constants are close to experimental values (see Table III) [33,36].

Our calculated direct band gaps at the X point (of PbTiO₃ and PbZrO₃) and at the Γ point (of other compounds) of cubic perovskites (at optimized lattice constant) in comparison with earlier theoretical and experimental results are presented in Fig. 2 [4,33,37–41]. SCAN gives a better estimation of band gaps of perovskites and other materials [20,21] compared to LDA [4,18,19]. LDA underestimates the band gaps by 40–50%. The band gaps in SCAN are also underestimated, but are modestly improved over LDA.

Next, we determine the effect of the exchange-correlation functional on vibrational properties which have important consequences for the finite-temperature properties of perovskites.

TABLE I. Optimized tetragonal lattice parameters (in Å) and z component of atomic displacements (from cubic to tetragonal phase) for BaTiO₃ and PbTiO₃ using the SCAN meta-GGA functional in comparison with earlier theoretical and experimental results [14]. Atomic displacements are given as a fraction of the c parameter.

Compound	Property	LDA [14]	PBE [14]	WC-GGA [14]	B3LYP [14]	SCAN	Expt. [14]
BaTiO ₃	a	3.954	4.013	3.982	3.996	3.985	3.986
	c/a	1.006	1.035	1.012	1.066	1.027	1.010
	d_z^{Ti}	0.011	0.018	0.013	0.019	0.016	0.015
	d_z^{O1}	−0.014	−0.039	−0.022	−0.057	−0.029	−0.023
	d_z^{O11}	−0.009	−0.022	−0.013	−0.031	−0.017	−0.014
PbTiO ₃	a	3.872	3.834	3.870	3.819	3.881	3.88
	c/a	1.041	1.221	1.086	1.277	1.110	1.063 (300 K)
	d_z^{Ti}	0.037	0.062	0.044	0.076	0.029	0.040
	d_z^{O1}	0.090	0.189	0.121	0.223	0.118	0.112
	d_z^{O11}	0.106	0.178	0.133	0.198	0.120	0.112

TABLE II. Optimized lattice parameters of orthorhombic and rhombohedral phases of BaTiO₃ and KNbO₃ using the SCAN meta-GGA functional in comparison with earlier theoretical and experimental results [29–32].

Compound	Phase	Lattice parameters	PBE-GGA	WC-GGA [32]	SCAN	Expt. [29–31]
BaTiO ₃	Rhombo	a (Å)	4.073		4.029	4.003
		α (°)	89.76		89.83	89.84
	Ortho	a (Å)	4.110		4.047	4.041
		b (Å)	3.996		3.983	3.982
		c (Å)	4.113		4.051	4.065
KNbO ₃	Rhombo	a (Å)	4.071	4.041	4.032	4.016
		α (°)	89.81	89.85	89.82	89.83
	Ortho	a (Å)	4.111	4.141	4.055	4.080
		b (Å)	3.988	3.980	3.969	3.973
		c (Å)	4.119	4.179	4.057	4.116

2. Vibrational properties

For the five-atom unit cell of cubic phase of perovskites, there are 12 optical phonon modes at the Γ point. Out of 12 optical modes, three triply degenerate phonon modes have Γ_{15} symmetry and one triply degenerate mode has Γ_{25} symmetry. The eigenvector of the phonon mode with Γ_{25} symmetry involves atomic displacements along the z direction as $v_z^A = 0$, $v_z^B = 0$, $v_z^{O_I} = \frac{1}{\sqrt{2}}$, $v_z^{O_{II}} = -\frac{1}{\sqrt{2}}$, and $v_z^{O_{III}} = 0$. Phonon modes with Γ_{15} symmetry are relevant to the ferroelectric

TABLE III. Elastic constants (in GPa) of cubic perovskites using the SCAN meta-GGA functional in comparison with earlier theoretically calculated values using LDA [4] and experimentally measured values [33,36].

Compound	Elastic constant	Method		
		SCAN	LDA [4]	Expt. [33,36]
BaTiO ₃	C_{11}	328	329	206
	C_{12}	118	117	140
	C_{44}	131	130	126
SrTiO ₃	C_{11}	374	389	316
	C_{12}	113	105	101
	C_{44}	120	155	119
CaTiO ₃	C_{11}	399	407	
	C_{12}	110	96	
	C_{44}	104	102	
PbTiO ₃	C_{11}	340	335	229
	C_{12}	135	146	101
	C_{44}	108	100	100
KNbO ₃	C_{11}	427	465	232
	C_{12}	83	67	90
	C_{44}	103	96	75
NaNbO ₃	C_{11}	472	482	230
	C_{12}	84	70	90
	C_{44}	77	78	76
PbZrO ₃	C_{11}	332	371	
	C_{12}	94	86	
	C_{44}	67	67	
BaZrO ₃	C_{11}	325	335	
	C_{12}	88	95	
	C_{44}	93	89	

transition [4]. One of the eigenvalues of the phonon modes with Γ_{15} symmetry of the cubic phase becomes negative (for the five-atom unit cell as experimental ground state), which indicates that the cubic phase is unstable. We have compared the optical phonon frequencies (see Table IV) obtained at the optimized lattice constant with earlier theoretical calculations based on LDA, GGA, and hybrid functionals and experimentally measured frequencies [14,42,43]. Our estimated zone-center optical phonon frequencies (TO1, TO2, TO3, and TO4) of BaTiO₃ and SrTiO₃ using SCAN are in excellent agreement (within 3% for BaTiO₃ and 8% for SrTiO₃) with experimental values and are better compared to earlier estimates calculated using LDA, GGA, and hybrid functionals [14]. For PbTiO₃, our calculated phonon frequencies differ by 19% from earlier theoretical results (using LDA, GGA, and hybrid functionals) [14]. Phonon frequencies of cubic PbTiO₃ cannot be readily compared with experimental values, as the literature is not available. SCAN predicts phonon frequencies much closer to the experimental values for cubic KNbO₃ compared to earlier LDA calculations [42]. Moreover, our predicted phonon frequencies (of BaTiO₃, SrTiO₃, and KNbO₃) are better

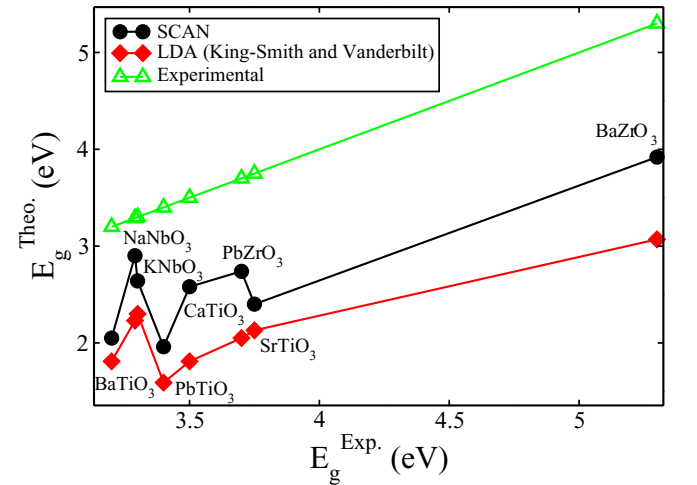


FIG. 2. Direct band gaps of eight perovskites in comparison with earlier theoretical results using LDA [4] and experimentally measured band gaps [33,37–41]. Experimentally measured band gaps of cubic KNbO₃ and NaNbO₃ are nearly equal.

TABLE IV. Predicted zone-center optical phonon frequencies (in cm^{-1}) of BaTiO_3 , PbTiO_3 , SrTiO_3 , and KNbO_3 at theoretical lattice constants in comparison with earlier theoretically calculated and experimentally measured frequencies [14,42,43].

Compound	Symmetry	Functional							Expt. [14,42,43]
		LDA [14,43]	WC-GGA [14]	B1-WC [14]	PBE [43]	HSE [43]	LDA-LAPW [42]	SCAN	
BaTiO_3	Γ_{15} (TO1)	75 <i>i</i>	128 <i>i</i>	145 <i>i</i>				196 <i>i</i>	
	Γ_{15} (TO2)	193	186	195				182	182
	Γ_{15} (TO3)	480	469	482				478	482
	Γ_{25} (TO4)	286	282	299				297	306
PbTiO_3	Γ_{15} (TO1)	127 <i>i</i>	132 <i>i</i>	146 <i>i</i>				147 <i>i</i>	
	Γ_{15} (TO2)	145	141	138				140	
	Γ_{15} (TO3)	515	510	513				530	
	Γ_{25} (TO4)	219	211	231				227	
SrTiO_3	Γ_{15} (TO1)	80			115 <i>i</i>	74 <i>i</i>		86	91 (297 K)
	Γ_{15} (TO2)	177			147	162		173	169 (297 K)
	Γ_{15} (TO3)	563			512	533		553	544 (297 K)
	Γ_{25} (TO4)	226			234	250		244	265 (297 K)
KNbO_3	Γ_{15} (TO1)	143 <i>i</i>					197 <i>i</i>	247 <i>i</i>	
	Γ_{15} (TO2)	188					170	207	198
	Γ_{15} (TO3)	506					473	483	521
	Γ_{25} (TO4)						243	272	280

than earlier theoretically calculated values using different functionals [14,42,43].

We now examine the eigenvalues of unstable phonon modes (TO1) with Γ_{15} symmetry (see Table V). We find that the value of the harmonic coupling parameter κ is positive (see Table V) for cubic BaZrO_3 , which assumes the cubic phase at all temperatures, and is consistent with the earlier LDA result and experimental findings [4]. The positive value of κ for SrTiO_3 is consistent with the antiferrodistortive transition associated with the phonon mode at $q \neq 0$. In contrast, earlier LDA results gave a negative value of κ for SrTiO_3 [4], while another LDA calculation with high plane-wave kinetic energy

cutoff (50 Ry) predicts a positive value ($0.096 \text{ eV}/\text{\AA}^2$) of κ of SrTiO_3 . For other compounds, the value of κ is found to be negative, which is in agreement with earlier theoretical results using LDA (see Table V). Overall, our calculated values of κ are more negative for BaTiO_3 , KNbO_3 , and NaNbO_3 compared to earlier LDA results, whereas they are more positive for other compounds, which are relevant for defining the potential energy surface [4].

The eigenvector of the soft mode of the cubic structure and its amplitude in the ferroelectric phase of BaTiO_3 (see Table VI) are comparable to the eigenvector obtained earlier

TABLE V. Harmonic (κ in $\text{eV}/\text{\AA}^2$), anharmonic (α and γ in $\text{eV}/\text{\AA}^4$), and strain-phonon coupling parameters (B_{1xx} , B_{1yy} , and B_{4yz} in $\text{eV}/\text{\AA}^2$) in comparison with earlier theoretically calculated values using LDA [4]. κ is the harmonic and α and γ are the anharmonic coupling coefficients (estimated by fitting the fourth-order polynomial in soft-mode amplitude) in the on-site energy.

Compound	Functional	Coupling coefficients							
		κ	α	γ	B_{1xx}	B_{1yy}	B_{4yz}	α'	γ'
BaTiO_3	SCAN	-1.92	112.73	-158.93	-225.76	-18.04	-20.93	57.92	-36.54
	LDA [4]	-1.68	110.32	-163.07	-210.32	-19.29	-7.72	60.68	-42.75
SrTiO_3	SCAN	0.49	21.37	-22.06	-64.64	-39.94	46.41	16.89	-44.47
	LDA [4]	-0.086	51.72	-65.85	-136.04	5.78	-10.61	32.06	-3.45
CaTiO_3	SCAN	-0.47	4.14	1.89	-49.97	-30.01	-10.81	2.59	2.52
	LDA [4]	-1.11	7.93	-2.07	-56.92	5.78	-9.65	4.48	21.03
PbTiO_3	SCAN	-0.77	6.79	-4.41	-66.37	-2.99	-23.25	1.59	1.79
	LDA [4]	-1.24	15.17	-15.51	-75.25	0.00	-2.89	7.58	8.62
KNbO_3	SCAN	-3.14	110.67	-149.97	-257.21	15.53	-3.28	57.58	-14.82
	LDA [4]	-1.49	130.32	-211.34	-290.40	31.84	-0.96	63.43	-38.27
NaNbO_3	SCAN	-1.53	28.27	-31.37	29.14	-44.96	6.66	24.82	-22.07
	LDA [4]	-1.19	57.92	-88.26	-164.98	48.24	0.00	32.06	-14.14
PbZrO_3	SCAN	-1.36	2.41	-0.17	33.67	5.49	-18.52	1.45	-3.75
	LDA [4]	-1.51	3.79	-4.48	-21.22	6.75	-0.96	3.10	-1.03
BaZrO_3	SCAN	1.82	1.69	2.41	16.98	29.62	19.39	0.55	-1.52
	LDA [4]	0.75	5.52	0.00	-45.34	6.75	-10.61	3.10	18.62

TABLE VI. Computed eigenvectors [ξ_z^{atom} (unitless)] and amplitudes of the soft modes of eight perovskites in comparison with earlier LDA results [4,44].

Compound	Method	ξ_z^A	ξ_z^B	$\xi_z^{O_{1,2}}$	$\xi_z^{O_3}$	Amplitude (bohr)
BaTiO ₃	SCAN	0.15	0.77	-0.18	-0.56	0.24
	LDA [4]	0.20	0.76	-0.21	-0.53	0.25
PbTiO ₃	SCAN	0.65	0.43	-0.40	-0.27	0.56
	LDA [4]	0.57	0.51	-0.41	-0.27	0.54
KNbO ₃	SCAN	0.12	0.80	-0.21	-0.50	0.30
	LDA [4]	0.18	0.80	-0.31	-0.37	0.22
SrTiO ₃	SCAN	0.52	0.57	-0.39	-0.30	0.0
	LDA [44]	0.49	0.60	-0.41	-0.27	
CaTiO ₃	SCAN	0.74	0.27	-0.42	0.17	0.38
	LDA [44]	0.68	0.36	-0.44	-0.17	
NaNbO ₃	SCAN	0.35	0.70	-0.38	-0.31	0.38
	LDA[44]	0.43	0.64	-0.43	-0.21	
PbZrO ₃	SCAN	0.81	0.09	-0.41	-0.09	1.06
	LDA [44]	0.77	0.15	-0.44	-0.04	
BaZrO ₃	SCAN	0.75	0.23	-0.43	-0.13	0.0
	LDA [44]	0.70	0.27	-0.46	-0.05	

using LDA [4], although the lattice constants obtained using the two functionals are quite different. On the other hand, the displacement of the Pb atom associated with the soft mode is large compared to the value obtained using LDA, although amplitudes of soft modes using the two different functionals are similar [4]. Eigenvectors of the soft modes of NaNbO₃ and CaTiO₃ obtained using the two functionals (SCAN and LDA) are slightly different from each other [4]. For other compounds, eigenvectors and amplitudes of the soft modes are comparable with the results estimated earlier using LDA [4]. Our calculated eigenvector of the soft mode of BaTiO₃ is similar to the eigenvector obtained using the WC-GGA functional [7].

Anharmonic coupling coefficients α and γ in the on-site energy are determined from the expressions for energy as a function of soft-mode amplitude (u) along the [001] and [111] directions (up to fourth-order terms in u) [4]:

$$E_{001}(u) = \kappa u^2 + \alpha u^4, \quad (1a)$$

$$E_{111}(u) = 3\kappa u^2 + (9\alpha + 3\gamma)u^4. \quad (1b)$$

The energies of unstrained cubic PbTiO₃ and BaTiO₃ as a function of soft-mode displacements are shown in Fig. 3. When strain is not applied, the rhombohedral phase has minimum energy for BaTiO₃ and PbTiO₃ (as shown in Fig. 3), consistent with earlier LDA results [4]. The depth of the double well (as shown in Fig. 3) is larger for PbTiO₃ compared to BaTiO₃ as the values of α and γ (obtained using SCAN) of PbTiO₃ are small (see Table V).

We compute strain-phonon coupling parameters to find the ground state of each oxide. Strain-phonon coupling parameters (B_{1xx} , B_{1yy} , and B_{4yz}) of the eight perovskites are determined by calculating the change in the values of κ with strain. Changes in the eigenvalues of an x -polarized soft mode (κ_x) with the applications of strains along the x (η_1) and y (η_2) directions give B_{1xx} and B_{1yy} , respectively (as shown in Fig. 4). To find the value of B_{4yz} , we calculate the change in the value of κ of the soft-mode distortion along the [111] direction with the change of shear strain (η_4). We

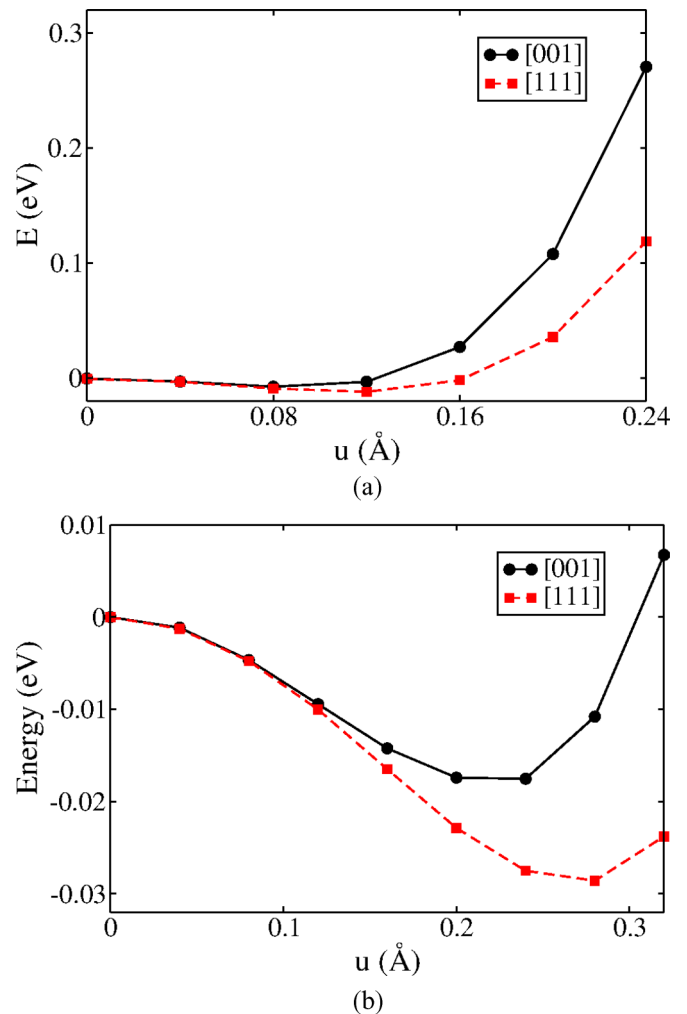


FIG. 3. Variations of total energies of unstrained (a) BaTiO₃ and (b) PbTiO₃ as a function of polar structural distortions (u) along the [001] and [111] directions, respectively, from SCAN.

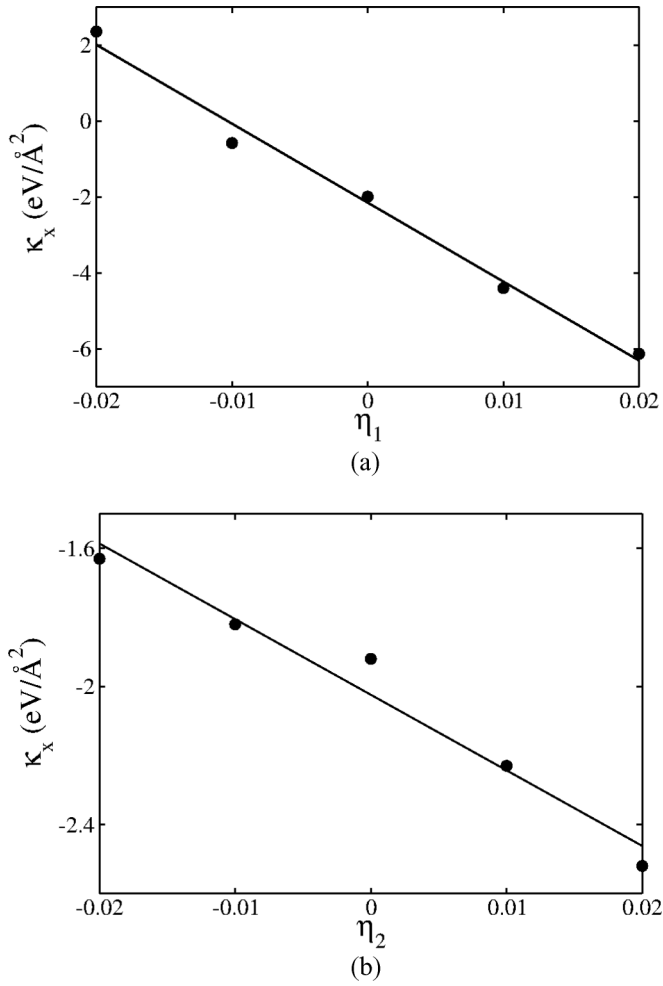


FIG. 4. Eigenvalue (κ_x) of x -polarized soft mode (with Γ_{15} symmetry) of BaTiO_3 as functions of strains applied along (a) the x (η_1) and (b) the y (η_2) directions, from SCAN.

notice that strain-phonon coupling parameters are sensitive to the exchange-correlation functional (see Table V). B_{1yy} and B_{4yz} coupling parameters of BaTiO_3 and PbTiO_3 mostly get affected by the exchange-correlation functional. For NaNbO_3 , PbZrO_3 , and BaZrO_3 , B_{1xx} even changes its sign with the change of exchange-correlation functional. We consider these calculated parameters to obtain the ground state of every compound, as discussed below.

Using the fourth-order expansion of energy as a function of soft-mode amplitude and strain, the energy differences between cubic (E_C), tetragonal (E_T), orthorhombic (E_O), and rhombohedral (E_R) phases are [4]

$$E_C - E_T = -\frac{\kappa^2}{4\alpha'}, \quad (2a)$$

$$E_C - E_O = -\frac{\kappa^2}{4\alpha' + \gamma'}, \quad (2b)$$

$$E_C - E_R = -\frac{\kappa^2}{4(\alpha' + \gamma'/3)}. \quad (2c)$$

Here, α' and γ' are the renormalized anharmonic coupling constants (as given in Eqs. (11b), (12b), and (13b) in Ref.

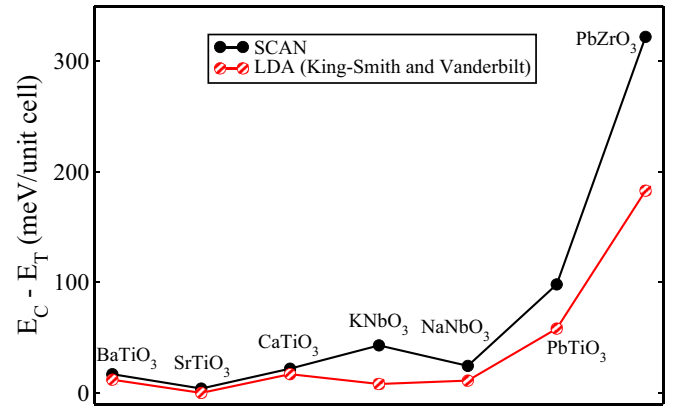


FIG. 5. Calculated energy difference (using fourth-order expansion of energy as a function of soft-mode amplitude) between cubic (E_C) and tetragonal (E_T) phases of perovskites in comparison with earlier theoretical results using LDA [4]. For CaTiO_3 , we employ the result of another theoretical calculation using LDA from Ref. [44].

[4]) which depend on elastic constants, strain-phonon coupling parameters, and bare anharmonic coupling constants (α and γ).

We find that the value of γ is typically negative, as shown in Table V. The introduction of strain switches the sign of γ in some cases, which highlights the importance of strain-phonon coupling. If κ is less than zero, the stability of tetragonal and rhombohedral ground states requires γ' to be greater-than and less-than zero, respectively [using Eqs. (2a)–(2c)]. Negative values of γ' of BaTiO_3 , KNbO_3 , NaNbO_3 , and PbZrO_3 mean that the ground state is rhombohedral, which is consistent with earlier theoretical results using LDA [4]. For PbTiO_3 and CaTiO_3 , the tetragonal state is the ground state as γ' is positive (consistent with earlier LDA results [4]). In addition, cubic phases of SrTiO_3 and BaZrO_3 have minimum energy as κ is positive. The experimentally observed ground states for SrTiO_3 , CaTiO_3 , and NaNbO_3 are the tetragonal (antiferrodistortive transition associated with oxygen octahedra rotation), orthorhombic (with 20 atoms in the unit cell), and monoclinic (20 atoms per unit cell) phase, respectively [4]. Hence, these cannot be explained using the fourth-order expansion of energy, which considers only the soft mode at the Γ point.

The calculated energy differences between the cubic and tetragonal phases [using Eq. (2a)] of BaTiO_3 , PbTiO_3 , and KNbO_3 are 16 meV/unit cell (12 meV/unit cell, LDA), 95 meV/unit cell (58 meV/unit cell, LDA) and 43 meV/unit cell (8 meV/unit cell, LDA), respectively (as shown in Fig. 5). For BaZrO_3 , the energy difference between the cubic and tetragonal phase is 1.3 eV/unit cell, which is much larger compared to the value (45 meV/unit cell) obtained using the parameters from earlier theoretical calculations using LDA [4]. For comparison of the energy difference between the cubic and tetragonal phases of CaTiO_3 , we use parameters from another calculation (with LDA) with a high plane-wave kinetic energy cutoff (50 Ry) [44]. SCAN produces deeper potential wells (energy as a function of soft-mode amplitude and strain) for all compounds, in comparison with earlier theoretical results using LDA [4,44]. The depths of the potential well

along the [110] and [111] directions [using Eqs. (2b) and (2c)] are 19 meV/unit cell and 20 meV/unit cell for BaTiO₃ and 46 meV/unit cell and 47 meV/unit cell for KNbO₃, respectively. Our calculated energy differences (orthorhombic and rhombohedral) are larger compared to the depth obtained using LDA-based parameters (BaTiO₃: 14 meV/unit cell and 15 meV/unit cell; KNbO₃: 9 meV/unit cell and 10 meV/unit cell). As the depths of double-well energy surfaces are believed to be underestimated in the LDA framework, the description of total-energy surfaces is improved by the accurate estimation of lattice constants using SCAN.

B. Finite-temperature properties

We now investigate the effect of the exchange-correlation functional on finite-temperature properties, i.e., transition temperatures of three compounds (BaTiO₃, PbTiO₃, and KNbO₃) whose ferroelectric transitions are associated with the soft mode at the Γ point.

1. Effective Hamiltonian

To predict the finite-temperature properties using MD simulation, we use an effective Hamiltonian [7,25]:

$$\begin{aligned}
H^{\text{eff}} = & \frac{M_{\text{dipole}}^*}{2} \sum_{\mathbf{R}, \alpha} \dot{u}_{\alpha}^2(\mathbf{R}) + \frac{M_{\text{acoustic}}^*}{2} \sum_{\mathbf{R}, \alpha} \dot{w}_{\alpha}^2(\mathbf{R}) + V^{\text{self}}(\{\mathbf{u}\}) \\
& + V^{\text{dpl}}(\{\mathbf{u}\}) + V^{\text{short}}(\{\mathbf{u}\}) + V^{\text{elas, homo}}(\eta_1, \dots, \eta_6) \\
& + V^{\text{elas, inho}}(\{\mathbf{w}\}) + V^{\text{coup, homo}}(\{\mathbf{u}\}, \eta_1, \dots, \eta_6) \\
& + V^{\text{coup, inho}}(\{\mathbf{u}\}, \{\mathbf{w}\}) - Z^* \sum_{\mathbf{R}} \mathcal{E} \cdot \mathbf{u}(\mathbf{R}), \quad (3)
\end{aligned}$$

where \mathbf{u} and \mathbf{w} are the local soft-mode amplitude vector (soft-mode displacement vector) and acoustic mode displacement vector (lattice Wannier mode [45]) of the unit cell at position \mathbf{R} , respectively ($\alpha = x, y, z$). η_1, \dots, η_6 are the homogeneous strain components. M_{dipole}^* and M_{acoustic}^* are effective masses associated with polar soft and acoustic modes, respectively. Z^* is the Born effective charge associated with the soft mode, and \mathcal{E} is the external electric field.

The third term in Eq. (3) represents local-mode self-energy [$V^{\text{self}}(\mathbf{u})$] [7]:

$$\begin{aligned}
V^{\text{self}}(\{\mathbf{u}\}) = & \sum_{\mathbf{R}} \kappa_2 u^2(\mathbf{R}) + \alpha u^4(\mathbf{R}) + \gamma [u_x^2(\mathbf{R}) u_y^2(\mathbf{R}) \\
& + u_y^2(\mathbf{R}) u_z^2(\mathbf{R}) + u_z^2(\mathbf{R}) u_x^2(\mathbf{R})] \\
& + k_1 u^6(\mathbf{R}) + k_2 \{u_x^4(\mathbf{R}) [u_y^2(\mathbf{R}) + u_z^2(\mathbf{R})] \\
& + u_y^4(\mathbf{R}) [u_z^2(\mathbf{R}) + u_x^2(\mathbf{R})] \\
& + u_z^4(\mathbf{R}) [u_x^2(\mathbf{R}) + u_y^2(\mathbf{R})]\} \\
& + k_3 u_x^2(\mathbf{R}) u_y^2(\mathbf{R}) u_z^2(\mathbf{R}) + k_4 u^8(\mathbf{R}), \quad (4)
\end{aligned}$$

where $u^2(\mathbf{R}) = u_x^2(\mathbf{R}) + u_y^2(\mathbf{R}) + u_z^2(\mathbf{R})$.

Equations (1a) and (1b) can be obtained from Eq. (4) by taking $\mathbf{u}(\mathbf{R}) = (0, 0, u)$ and $\mathbf{u}(\mathbf{R}) = (u, u, u)$ and replacing κ_2 to κ and truncating the polynomial in u at the fourth-order terms. The fourth and fifth terms in Eq. (3) represent long-range dipole-dipole interaction and short-range harmonic interaction

between optical displacements [$\mathbf{u}(\mathbf{R})$] up to third nearest neighbors. Terms containing acoustic mode displacement vector [$\mathbf{w}(\mathbf{R})$] have been integrated out by minimizing Eq. (3) with respect to [$\mathbf{w}(\mathbf{R})$] [25]. The sixth and eighth terms in Eq. (3) are the elastic energy and coupling between homogeneous strain and optical mode (\mathbf{u}), which have been determined here by using the coupling constants [elastic constant ($C_{\alpha\beta\gamma\delta}$) and strain-phonon coupling ($B_{i\alpha\beta}$) parameters], as discussed in the earlier section. We did not include the effect of external electric field.

The short-range and long-range interaction parameters determine the energy (or frequency) of the soft mode at high-symmetry points other than Γ . We determine phonon spectra at X , M , and R points of the Brillouin zone of BaTiO₃, PbTiO₃, and KNbO₃ to calculate the short-range interaction parameters. These phonon calculations (at X , M , and R points) were performed with $(1 \times 1 \times 2)$, $(\sqrt{2} \times \sqrt{2} \times 1)$, and $(\sqrt{2} \times \sqrt{2} \times \sqrt{2})$ supercells containing 10 atoms each, respectively. In addition, we calculate phonon modes at the center of the Σ axis ($q = (110)\frac{\pi}{2a}$) by considering the $2\sqrt{2} \times 1 \times \sqrt{2}$ supercell with 20 atoms for PbTiO₃. We should note that these calculations use the cubic structure of these compounds. The long-range dipole-dipole interaction is proportional to Z^{*2}/ϵ_{∞} , where Z^* is the mode effective charges associated with the soft mode and ϵ_{∞} is the dielectric constant [10]. Our calculated values of Z^* are 10.16 (BaTiO₃), 9.37 (PbTiO₃), and 11.52 (KNbO₃), M^* are 37.5 amu (BaTiO₃), 102.6 amu (PbTiO₃), and 65.4 amu (KNbO₃), and ϵ_{∞} are 6.27 (BaTiO₃), 7.95 (PbTiO₃), and 5.492 (KNbO₃). While the SCAN meta-GGA estimates of Z^{*2}/ϵ_{∞} are within 10% of the LDA estimates, they are closer (within 5%) to the Wu-Cohen-functional-based estimates available for KNbO₃ and BaTiO₃ [7,32]. We consider local modes with Ti- and Nb-centered atomic displacements (at Γ , X , M , and R points) to study the phase transitions in BaTiO₃ and KNbO₃ [45]. However, Pb-centered local modes (at Γ , X , M , and R points) have been used here to study the phase transition in PbTiO₃ [8]. For studying phase transitions, we use the eigenvalues of doubly degenerate modes with X_5 (X'_5 mode for PbTiO₃) and M'_5 (M'_5 mode for PbTiO₃) symmetries, nondegenerate modes with X_1 (X'_2 mode for PbTiO₃) and M'_3 (M'_2 mode for PbTiO₃) symmetries, and triply degenerate mode with R'_{25} (R_{15} mode for PbTiO₃) symmetry of KNbO₃ and BaTiO₃. We also take into account one Pb-based optical phonon mode at the $(110)\frac{\pi}{2a}$ point of PbTiO₃. The local (κ_2) and short-range interaction parameters (j_1, \dots, j_7) are determined by using the eigenvalues (ω) of these selected phonon modes and solving the linear equations as given in Refs. [7,8,10].

The total harmonic interaction (long- and short-range) matrix $\Phi^{\text{quad}}(k)$ is analyzed using FERAM [7,26] to get the model phonon dispersion of BaTiO₃ (see Fig. 6), which is similar to the dispersion obtained in earlier simulations using WC-GGA-based parameters [7]. The short-range interaction gives the most unstable mode at the X point [see Fig. 6(a)]. The dipole-dipole long-range interaction term results in a cell-doubling state due to the strongest instability at the M point [25]. The long-range dipole-dipole interaction splits the longitudinal and transverse optical phonon modes at the Γ point [see Fig. 6(b)] and the splitting in ω is proportional to Z^{*2}/ϵ_{∞} . However, the competing short- and long-range

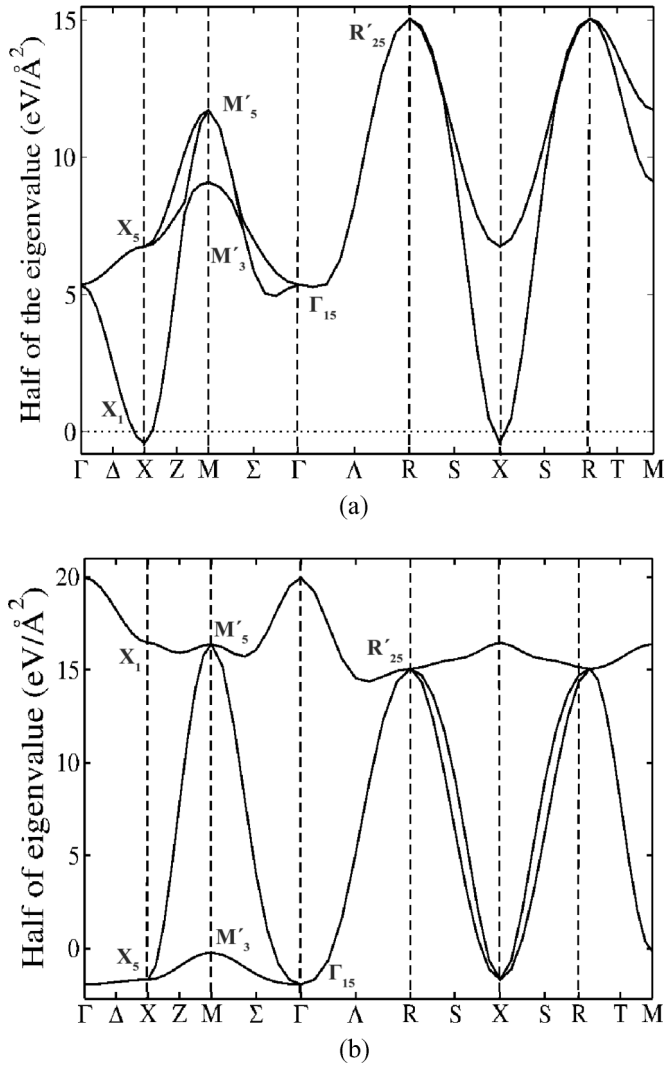


FIG. 6. Half of the eigenvalues of (a) short-range interaction matrix and (b) total (long- and short-range) interaction matrix (Eqs. (12) and (13) in Ref. [25]) along the high-symmetry directions of BaTiO₃.

interactions together give the strongest instability at the Γ point. The short-range interaction parameters of BaTiO₃, PbTiO₃, and KNbO₃ are given in Table VII. For BaTiO₃, the short-range interaction parameters are comparable to the parameters based on earlier calculations using WC-GGA. As LDA underestimates lattice constants, the local (κ_2) and short-range interaction parameters (j_2 , j_5 , and j_7) calculated earlier using LDA are different from our estimates. The short-range interaction parameters of PbTiO₃ obtained using SCAN are similar to the values obtained using LDA at the experimental lattice constant (partly justifying this approximation in Ref. [8]) [8,46]. For KNbO₃, local (κ_2) and short-range interaction parameters (j_1 , j_2 , and j_4) are different from earlier theoretical results using WC-GGA [26].

2. MD simulations

Using a SCAN-based parametrized effective Hamiltonian [truncating the local-mode self-energy up to fourth-order terms in u in Eq. (4)] [10,25], we perform heating-up and

TABLE VII. Calculated local and short-range interaction parameters (in eV/Å²) of BaTiO₃, PbTiO₃, and KNbO₃ in comparison with earlier theoretical results determined using LDA [7,8,46] and WC-GGA [7,26] functionals.

Compound	Parameter	SCAN	LDA [7,8,46]	WC-GGA [7,26]
BaTiO ₃	κ_2	8.31	5.52	8.53
	j_1	-2.54	-2.65	-2.08
	j_2	-0.82	3.906	-1.12
	j_3	0.78	0.90	0.68
	j_4	-0.52	-0.79	-0.61
	j_5	0.0	0.56	0.0
	j_6	0.32	0.36	0.27
PbTiO ₃	κ_2	1.36	1.17	
	j_1	-1.36	1.17	
	j_2	4.84	-1.35	
	j_3	0.45	4.98	
	j_4	-0.11	0.22	
	j_5	0.60	-0.018	
	j_6	-0.09	-0.083	
KNbO ₃	κ_2	10.06		11.42
	j_1	-5.06		-3.27
	j_2	1.87		-1.15
	j_3	1.09		1.10
	j_4	0.07		-0.66
	j_5	0.0		0.0
	j_6	0.43		0.30
	j_7	0.0		0.0

cooling-down molecular dynamics simulations for BaTiO₃, PbTiO₃, and KNbO₃ to estimate T_C . We define T_C for the phase transition $P \leftrightarrow Q$ to be the mean of the transition temperatures for $P \rightarrow Q$ and $Q \rightarrow P$. Simulated lattice parameters of these compounds as a function of temperature are presented in Fig. 7. For BaTiO₃ and KNbO₃, we find three transitions: from cubic (C) to tetragonal (T), from tetragonal (T) to orthorhombic (O), and from orthorhombic (O) to rhombohedral (R), which are consistent with the experimental observations [42,47]. We find a single structural transition from the cubic to tetragonal phase in PbTiO₃.

Our predicted transition temperatures of BaTiO₃ (see Table VIII) are T_C (C \leftrightarrow T) = 213 K, T_C (T \leftrightarrow O) = 141 K, and T_C (O \leftrightarrow R) = 111 K [see Fig. 7(a)]. The T_C of BaTiO₃ are underestimated by up to 65% with respect to the experimental transition temperatures [47]. However, our T_C are 45% higher than earlier results obtained using LDA at zero pressure [7]. The accurate determination of total-energy surfaces using SCAN gets reflected in the estimates of the transition temperatures. The rhombohedral to orthorhombic transition temperature is improved compared to earlier LDA and WC-GGA results at zero pressure [7]. The T_C of the transitions from the orthorhombic phase to tetragonal phase and the tetragonal to cubic phase are 29% lower than the T_C obtained with parameters obtained using the WC-GGA functional at zero pressure [7]. The c/a ratio of the tetragonal phase obtained using the SCAN-based parametrized effective Hamiltonian is 1.009 at 150 K, which agrees very well with

TABLE VIII. Estimated T_C of BaTiO₃, PbTiO₃, and KNbO₃ in comparison with earlier theoretical [7,8,46] and experimental T_C [26,42,47–49].

Compound	Exchange-correlation functional	R ↔ O	O ↔ T	T ↔ C
BaTiO ₃	SCAN	111 K	141 K	213 K
	SCAN (including anharmonic coupling between phonons)	230 K	278 K	375 K
	LDA, 0.0 GPa [7]	95 K	110 K	137 K
	LDA, −5.0 GPa [7]	210 K	245 K	320 K
	WC-GGA, 0.0 GPa [7]	102 K	160 K	288 K
	WC-GGA, −2.0 GPa [7]	117 K	218 K	408 K
	WC-GGA, −0.005T GPa [7]	103 K	187 K	411 K
	Expt. [47]	183 K	278 K	403 K
KNbO ₃	SCAN	160 K	225 K	540 K
	SCAN (including anharmonic coupling between phonons)	160 K	230 K	565 K
	LDA (experimental lattice constant) [48]	210 K	260 K	370 K
	WC-GGA [26], 0.0 GPa	177 K	310 K	660 K
	WC-GGA [26], −0.001T GPa	175 K	323 K	703 K
	Expt. [42]	210 K	488 K	701 K
PbTiO ₃	SCAN			630 K
	SCAN (including anharmonic coupling between phonons)			675 K
	LDA (experimental lattice constant) [8,46]			635 K
	Expt. [49]			763 K

the experimental value (1.01) [14]. Earlier MD simulations using the WC-GGA-based parameters gave the c/a ratio of the tetragonal phase (1.017 at 155 K) higher than the experimental value [7,14]. It has been observed from earlier results that the tetragonal to cubic transition temperature changes drastically by the application of negative pressure, whereas the two other T_C do not depend strongly on pressure. As our calculated strain-phonon coupling parameters are distinct from those in earlier works ($B_{1xx} = -185.33 \text{ eV}/\text{\AA}^2$ and $B_{1yy} = -3.28 \text{ eV}/\text{\AA}^2$) using the WC-GGA functional, the transition temperatures estimated with these two functionals are different [7].

Our estimated three transition temperatures (see Table VIII) of KNbO₃ (O ↔ R = 160 K, T ↔ O = 225 K, and C ↔ T = 540 K) using the SCAN-based parameters [see Fig. 7(b)] are underestimated compared to the experimental T_C (O ↔ R = 210 K, T ↔ O = 488 K, and C ↔ T = 701 K) with the largest error for the T ↔ O transition [42]. Values of T_C (T ↔ O) and T_C (O ↔ R) calculated here are slightly underestimated compared to earlier LDA results at the experimental lattice constant [48]. However, our calculated T_C (C ↔ T) is much larger compared to earlier LDA results at the experimental lattice constant [48]. On the other hand, our predicted transition temperatures are lower than the calculated T_C using the WC-GGA functional at zero pressure [26]. The optimized lattice parameter of cubic KNbO₃ using SCAN is similar to the earlier computed value using the WC-GGA functional [26]. However, the inclusion of higher-order (greater than 4) on-site anharmonic coupling parameters and drastically different strain-phonon coupling parameters ($B_{1xx} = -220.45 \text{ eV}/\text{\AA}^2$ and $B_{1yy} = 31.35 \text{ eV}/\text{\AA}^2$) in earlier WC-GGA calculations result in different values of T_C compared to our estimated values [26]. We must note that application of negative pressure (using the WC-GGA-based effective Hamiltonian for BaTiO₃ and KNbO₃) does not affect the two lowest structural transition

temperatures (O ↔ R and T ↔ O), whereas only T_C (C ↔ T) is a strong function of pressure [7,26]. The WC-GGA functional has been constructed with a particular focus on ferroelectric materials [7,17]. On the other hand, the SCAN meta-GGA functional is universal as it is applicable for all diversely bonded materials but might fail to precisely determine one specific property of a particular type of material. However, SCAN removes the typical error in estimating T_C arising from the underestimation of lattice constant.

For PbTiO₃, we find a cubic to tetragonal phase transition at 630 K [see Fig. 7(c)], which is slightly lower than the experimental $T_C = 763 \text{ K}$ (see Table VIII). However, our predicted T_C is close to earlier calculated T_C (635 K) based on LDA parameters at the experimental lattice constant [49]. The tetragonal c/a ratio at 0 K (obtained by extrapolating lattice parameters) is 1.104, which is overestimated compared to the experimental value (1.071 at 0 K) [14]. It is clear that SCAN-based predictions of the transition temperatures of the three oxides improve over those of LDA-based parameters [8,46].

The discrepancies between our calculated T_C and experimental T_C have a contribution from the neglect of the anharmonic coupling between the soft mode and higher-energy phonon modes, as the error in the lattice constant has been minimized using the SCAN meta-GGA functional. The effect of including anharmonic coupling between soft and higher-energy modes on finite-temperature properties will be discussed in the following section.

C. Anharmonic coupling between phonons

We find that the depths of the double-well potentials of BaTiO₃, PbTiO₃, and KNbO₃ (along the [001] direction) obtained directly from DFT calculations ($E_{\text{cubic}} - E_{\text{tetragonal}} = 25 \text{ meV/unit cell}$ for BaTiO₃, 123 meV/unit cell for PbTiO₃, and 47 meV for KNbO₃) and from the effective Hamiltonian

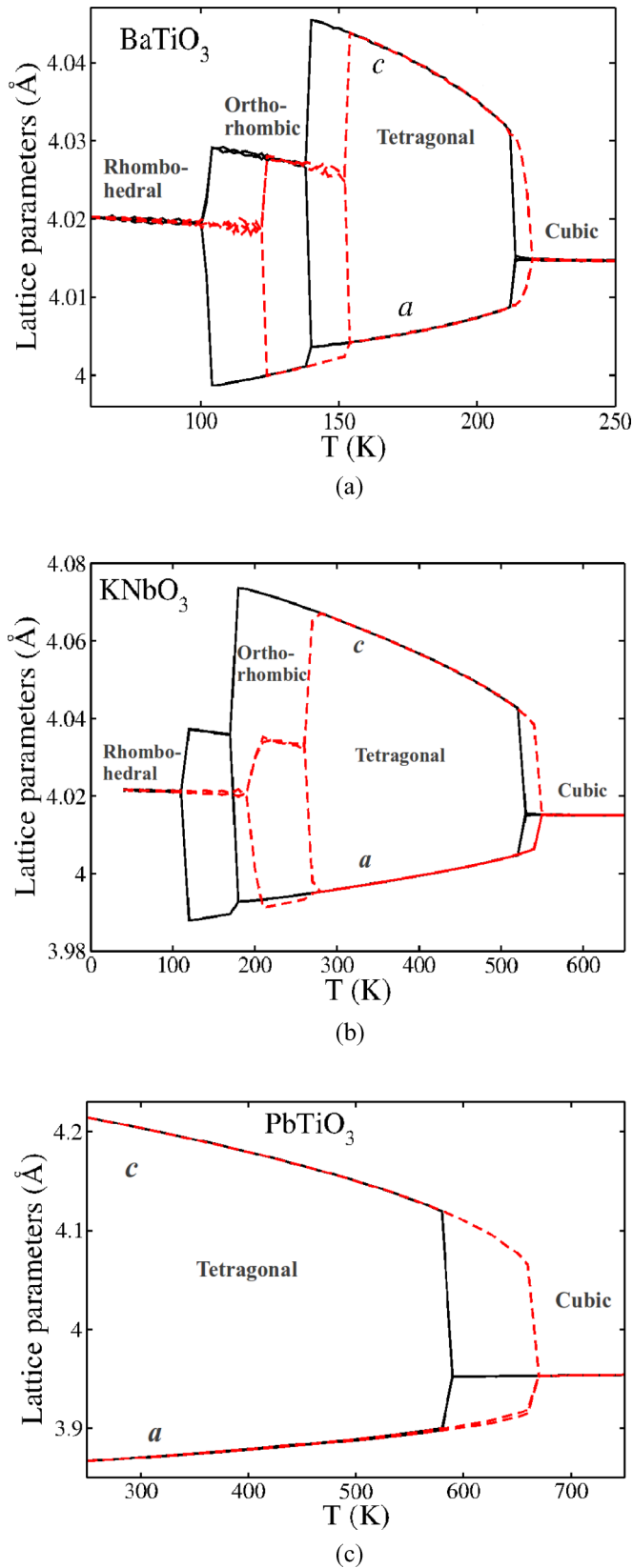


FIG. 7. Simulated temperature dependence of lattice parameters of (a) BaTiO₃, (b) KNbO₃, and (c) PbTiO₃ at zero pressure. Red (dashed) and black (solid) lines represent heating and cooling curves, respectively.

[Eq. (2a)] written as a fourth-order expansion (16 meV/unit cell for BaTiO₃, 95 meV/unit cell for PbTiO₃, and 43 meV for KNbO₃) are different. This difference in energies highlights the presence of anharmonic coupling between the soft mode and other higher-energy optical phonon modes.

To identify higher-energy optical phonon modes responsible for the phase transition, we define a vector, given as

$$\vec{S} = \vec{f} - (\vec{f} \cdot \hat{e}_{\text{soft}})\hat{e}_{\text{soft}}, \quad (5)$$

where \hat{e}_{soft} is the soft-mode eigenvector and \vec{f} is the ferroelectric distortion given as the atomic displacement vector from the cubic to tetragonal phase. Phonon modes having Γ_{15} symmetry with frequencies 182 cm⁻¹ (for BaTiO₃), 140 cm⁻¹ (for PbTiO₃), and 207 cm⁻¹ (for KNbO₃) show strong overlap (0.79 for BaTiO₃, 0.55 for PbTiO₃, and 0.52 for KNbO₃) with \vec{S} . We find higher-energy optical phonon modes with Γ_{15} symmetry (478 cm⁻¹ for BaTiO₃, 530 cm⁻¹ for PbTiO₃, and 483 cm⁻¹ for KNbO₃) contributing sizably to the ferroelectric distortion of the cubic phase.

To model the lowest-order coupling between these Γ_{15} modes, we write the total energy (along the [001] direction) as a function of soft mode (u) and higher-energy modes v_1 (182 cm⁻¹ for BaTiO₃, 140 cm⁻¹ for PbTiO₃, and 207 cm⁻¹ for KNbO₃) and v_2 (478 cm⁻¹ for BaTiO₃, 530 cm⁻¹ for PbTiO₃, and 483 cm⁻¹ for KNbO₃) by expanding it as a symmetry-invariant Taylor series expansion up to eighth order in u and second order in v_1 and v_2 with respect to the cubic phase using ISOTROPY [50]:

$$E(u, v_1, v_2) = \kappa u^2 + \alpha' u^4 + k_1 u^6 + k_4 u^8 + \kappa_{v_1} v_1^2 + e_1 u^3 v_1 + f_1 u^2 v_1^2 + \kappa_{v_2} v_2^2 + e_2 u^3 v_2 + f_2 u^2 v_2^2. \quad (6)$$

We have not considered the cubic coupling terms in higher-energy phonon modes as their contributions to the energy are less significant. e_1 and e_2 have been determined by projecting forces (arising due to the freezing of the soft mode) on v_1 and v_2 , as shown in Figs. 8(a) and 8(b), respectively. f_1 and f_2 coupling terms have been evaluated by calculating the eigenvalues of v_1 and v_2 modes as a function of amplitude of the soft mode (u), shown in Figs. 8(c) and 8(d), respectively. Such anharmonic coupling between the soft mode and higher-energy optical phonon modes was ignored in the earlier model Hamiltonian [Eq. (4)].

Minimizing the total energy [Eq. (6)] with respect to v_1 and v_2 , the resulting $v_{1,\text{min}}$ and $v_{2,\text{min}}$ are

$$v_{1,\text{min}} \approx -\frac{e_1 u^3}{2\kappa_{v_1}} \left(1 - \frac{f_1}{\kappa_{v_1}} u^2\right), \quad (7a)$$

$$v_{2,\text{min}} \approx -\frac{e_2 u^3}{2\kappa_{v_2}} \left(1 - \frac{f_2}{\kappa_{v_2}} u^2\right). \quad (7b)$$

The renormalized form of the total energy as a function of u is obtained by substituting $v_{1,\text{min}}$ and $v_{2,\text{min}}$ in Eq. (6):

$$\begin{aligned} E(u) &= \kappa u^2 + \alpha' u^4 + \left(k_1 - \frac{e_1^2}{4\kappa_{v_1}} - \frac{e_2^2}{4\kappa_{v_2}}\right) u^6 \\ &+ \left(k_4 - \frac{e_1^2 f_1}{4\kappa_{v_1}^2} - \frac{e_2^2 f_2}{4\kappa_{v_2}^2}\right) u^8 \\ &= \kappa u^2 + \alpha' u^4 + k'_1 u^6 + k'_4 u^8. \end{aligned} \quad (8)$$

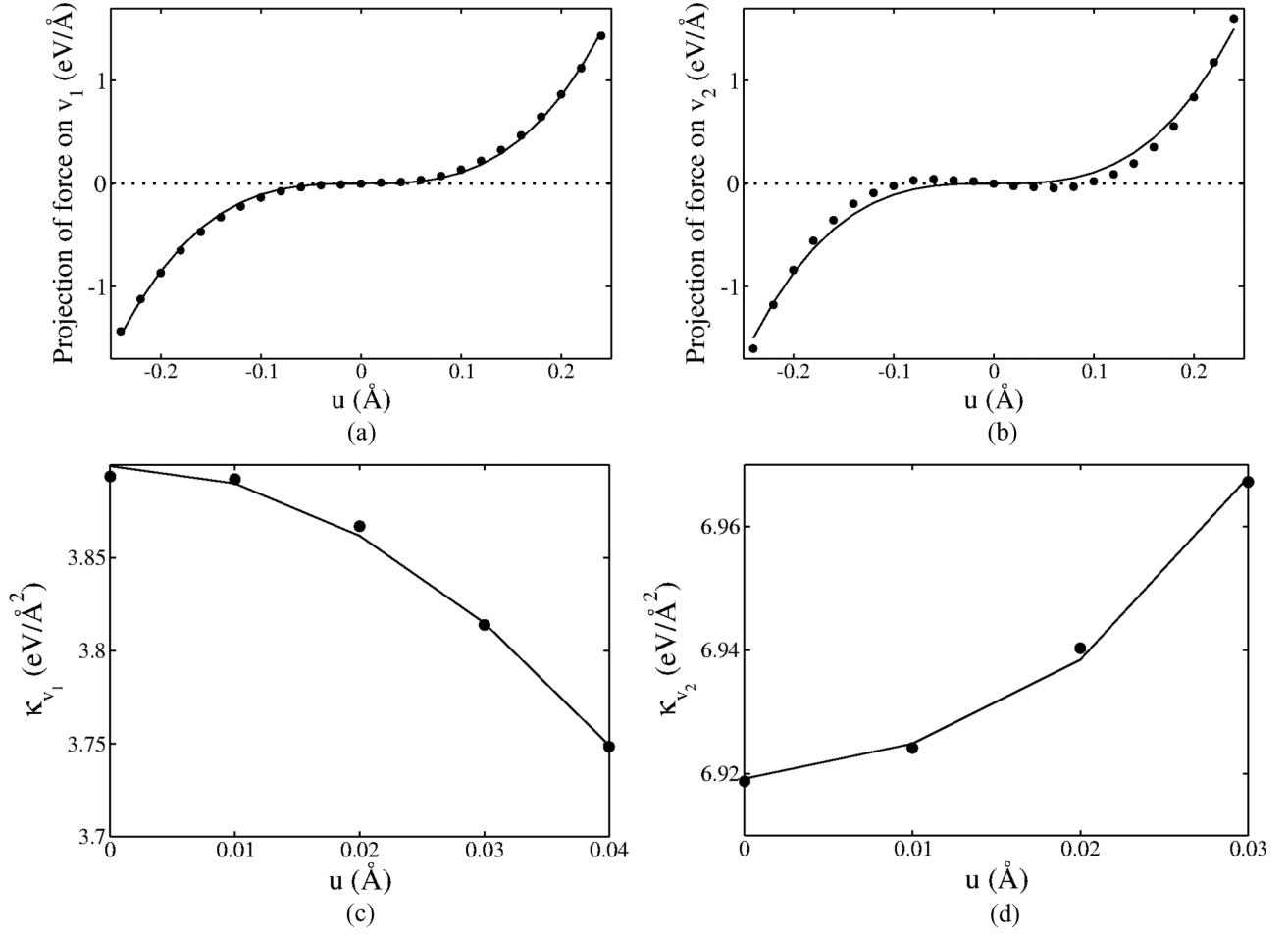


FIG. 8. Projection of forces arising due to the freezing of the soft mode on the (a) v_1 and (b) v_2 modes of BaTiO₃. Eigenvalues of the (c) v_1 and (d) v_2 modes as a function of soft-mode amplitude (u).

The fourth-order coupling terms between phonon modes modify the terms associated with sixth and eighth order in soft-mode displacement.

The expressions for total energies as a function of u along the [110] and [111] directions are [7]

$$E_{110}(u) = \kappa u^2 + \left(\alpha' + \frac{1}{4}\gamma'\right)u^4 + \left(k_1' + \frac{1}{4}k_2\right)u^6 + k_4'u^8, \quad (9a)$$

$$E_{111}(u) = \kappa u^2 + \left(\alpha' + \frac{1}{3}\gamma'\right)u^4 + \left(k_1' + \frac{2}{9}k_2 + \frac{1}{27}k_3\right)u^6 + k_4'u^8. \quad (9b)$$

For BaTiO₃, the values of the coupling constants are 3.95 eV/Å² (k_{v_1}), 6.85 eV/Å² (k_{v_2}), 107.91 eV/Å⁴ (e_1), 107.22 eV/Å⁴ (e_2), -92.74 eV/Å⁴ (f_1), 52.75 eV/Å⁴ (f_2), -325.24 eV/Å⁶ (k_1), and 2196.59 eV/Å⁸ (k_4). We have also determined the sixth-order terms k_2 (407.79 eV/Å⁶) and k_3 (1286.21 eV/Å⁶) to define the potential energy surface for distortions along the [110] and [111] directions [using Eqs. (9a) and (9b)].

When the double-well energy functions (along the [111] and [001] directions) are fitted with an eighth-order polynomial, the values of α and γ change to 126.18 eV/Å⁴ and -171.69 eV/Å⁴, respectively. However, the addition of sixth- and eighth-order terms (without including coupling between soft polar and higher-energy modes) does not affect the well depth and transition temperatures. The calculated energy difference between the cubic and tetragonal phases using Eq. (8) is 24 meV, which is closer to the value obtained from DFT calculations (25 meV).

To investigate the effect of changing the depth of the double-well potential energy on finite-temperature properties, we calculate the transition temperatures of BaTiO₃ considering our generalized effective Hamiltonian [Eqs. (8), (9a), and (9b)]. Our simulated three transition parameters (see Table VIII) using the new parameters (k_1' and k_4') are 230 K (O \leftrightarrow R), 278 K (R \leftrightarrow T), and 375 K (T \leftrightarrow C), as shown in Fig. 9(a). The tetragonal to cubic transition temperature increases by 57% from the value (217 K) obtained without including the coupling between soft mode and higher-energy modes. The simulated value of the c/a ratio at 300 K of the tetragonal phase is 1.014, which is slightly overestimated compared to the experimental value (1.010), as expected [14]. Here, we did not include the anharmonic coupling between phonons to modify

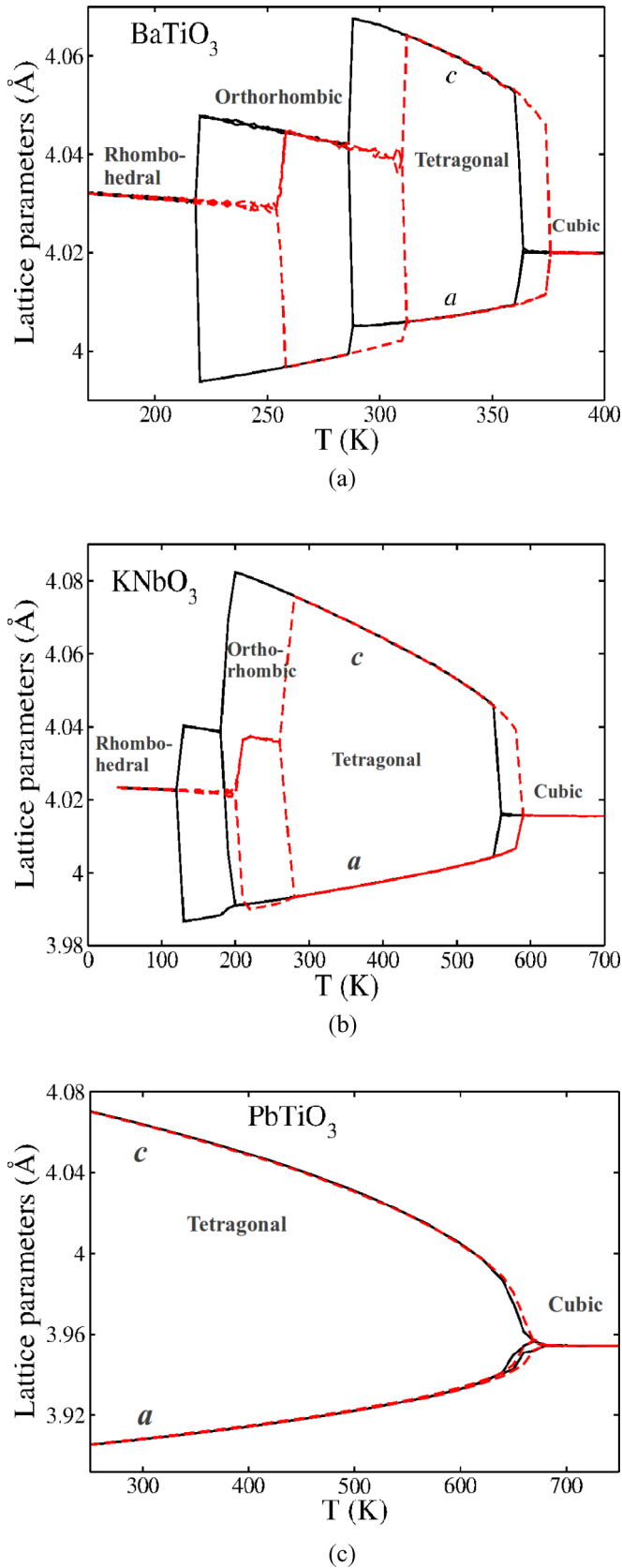


FIG. 9. Estimated T_C of (a) BaTiO_3 , (b) KNbO_3 , and (c) PbTiO_3 including the fourth-order coupling between soft and higher-energy phonon modes. Heating and cooling curves are indicated by red (dashed) and black (solid) lines, respectively.

the k_2 and k_3 parameters, which will precisely determine the depth of the energy well along the [111] and [110] directions. This leads to the slight overestimation of two lower T_C .

Similarly, the depth of the potential well of the tetragonal state in the model of KNbO_3 increases by 9 meV [from the value of 43 meV obtained using Eq. (2a)] after including the effects of anharmonic coupling between soft-mode and higher-energy phonons ($k_{v_1} = 3.27 \text{ eV/\AA}^2$, $k_{v_2} = 7.17 \text{ eV/\AA}^2$, $e_1 = 0.2 \text{ eV/\AA}^4$, $e_2 = -139.2 \text{ eV/\AA}^4$, $f_1 = -135.5 \text{ eV/\AA}^4$, $f_2 = -138.3 \text{ eV/\AA}^4$, $k_1 = -464.3 \text{ eV/\AA}^6$, $k_4 = 1658 \text{ eV/\AA}^8$, $k_2 = 550 \text{ eV/\AA}^6$, and $k_3 = 1347 \text{ eV/\AA}^6$). It is slightly overestimated compared to the energy well depth calculated using DFT calculations (47 meV). The values of α and γ changes to 127 eV/\AA^4 and -166 eV/\AA^4 , respectively (which does not affect the T_C when anharmonic coupling between phonons is not included), when the double-well energy functions are fitted with an eighth-order polynomial. The calculated values of T_C of KNbO_3 using our generalized model Hamiltonian with SCAN-based parameters are T_C ($\text{C} \leftrightarrow \text{T}$) = 565 K, T_C ($\text{T} \leftrightarrow \text{O}$) = 230 K, and T_C ($\text{O} \leftrightarrow \text{R}$) = 160 K [see Table VIII and Fig. 9(b)]. We notice an increase in the tetragonal to cubic transition temperature by 25 K from the value (540 K) calculated earlier here, while the other two T_C almost remain unaltered.

Furthermore, we have calculated anharmonic coupling parameters between the soft mode and the other two optical phonon modes ($\omega_{v_1} = 140 \text{ cm}^{-1}$ and $\omega_{v_2} = 530 \text{ cm}^{-1}$) with Γ_{15} symmetry ($\kappa_{v_1} = 2.70 \text{ eV/\AA}^2$, $\kappa_{v_2} = 7.91 \text{ eV/\AA}^2$, $e_1 = 41.02 \text{ eV/\AA}^4$, $e_2 = 28.61 \text{ eV/\AA}^4$, $f_1 = -12.75 \text{ eV/\AA}^4$, $f_2 = -18.27 \text{ eV/\AA}^4$, $k_1 = -1.97 \text{ eV/\AA}^6$, and $k_4 = 13.64 \text{ eV/\AA}^8$) of PbTiO_3 . The value of α changes slightly (6.52 eV/\AA^4), when the potential energy surface along the [001] direction is fitted with an eighth-order polynomial and it does not affect the well depth and transition temperature. The evaluated energy difference between the cubic and tetragonal phases using Eq. (8) is 151 meV, which is slightly overestimated compared to the value (123 meV) obtained using the DFT calculation. After including anharmonic couplings between soft and higher-energy modes, we find an increase in T_C to 675 K [see Fig. 9(c)] from the value (630 K) calculated earlier here (see Table VIII). The c/a ratio at 0 K (obtained by extrapolating lattice parameters) is 1.053, which is in close agreement with the experimental value (1.071 at 0 K), but some errors are expected from approximately integrating out the higher-energy optic phonons [14]. Overall, our model based on the parameters calculated using SCAN precisely determines the depth of the potential well along the [001] direction, and gives a better estimation of the T_C and c/a ratios of the tetragonal phases of BaTiO_3 and PbTiO_3 .

IV. SUMMARY

We demonstrated consistent improvement in the theoretical prediction of structural parameters of the eight cubic perovskite oxides using the SCAN meta-GGA functional relative to LDA or GGA. In addition, estimates of band gaps of perovskite oxides typically increase and modestly improve over the earlier estimates of band gaps obtained with

LDA. Accurate structural parameters given by the SCAN meta-GGA functional allow estimation of more realistic total-energy surfaces of cubic perovskites as a function of soft-mode amplitude, which are relevant to the temperature-dependent structural phase transition. Our predicted zone-center optical phonon (stable modes) frequencies using the SCAN meta-GGA functional are in better agreement with the experimentally observed frequencies compared to the values using other functionals. Elastic constants and eigenvectors of soft modes are weakly dependent on the choice of exchange-correlation energy functional. For BaTiO₃, PbTiO₃, and KNbO₃, the strain-phonon coupling parameter B_{4yz} and anharmonic coupling terms and eigenvalues of soft modes get significantly altered by the SCAN meta-GGA exchange-correlation functional. The depths of the double-well energy surfaces of the polar distortions along the [001], [110], and [111] directions determined using the SCAN meta-GGA functional are notably enhanced relative to the depth obtained earlier using LDA.

As a consequence of these improvements, estimates of T_C of all the structural transitions in BaTiO₃ and PbTiO₃ are closer to experiment than those of the earlier LDA results. In particular, analysis of temperature-dependent transitions can be carried out with the SCAN meta-GGA-based energy surface without having to use negative pressure to compensate for error in lattice constants (e.g., in LDA). We have quantified the consequences of truncation of the subspace of the effective Hamiltonian using the lowest-order coupling between soft

and higher-energy optic modes with Γ_{15} symmetry to the estimation of T_C . The fourth-order anharmonic coupling between the soft polar mode and higher-energy optical modes in BaTiO₃ and PbTiO₃ causes the increase in the depth of the potential well, and consequently enhances the estimated T_C (Figs. 7 and 9, and Table VIII). At the interfaces in heterostructures or superlattices based on perovskite oxides, details of the atomic-scale structure depend on the mismatch between lattice constants, and electronic band offsets depend on band gaps. Since estimates of both lattice constants and band gap are consistently improved with SCAN meta-GGA calculations, we expect SCAN meta-GGA to be very effective in simulations of perovskite heterostructures.

ACKNOWLEDGMENTS

A.P. is thankful for financial support from the research fellowship from the Department of Science and Technology, India, and Thematic Unit of Excellence on Computational Material Science, JNCASR, India, for computational resources. U.V.W. is thankful for support from a J. C. Bose National Fellowship of the Department of Science and Technology, Government of India. The work of J.S. and J.P.P. (who contributed to the design of the project and the writing) is supported by the Centre for the Computational Design of Functional Layered Materials, an Energy Frontier Research Centre funded by the U.S. Department of Energy, Office of Science, Basic Energy Sciences, under Award No. DE-SC0012575.

-
- [1] M. Lines and A. Glass, *Principles and Applications of Ferroelectrics and Related Materials*, International series of Monographs on Physics (OUP, Oxford, 1977).
 - [2] R. Waser, *Nanoelectronics and Information Technology* (Wiley, New York, 2012).
 - [3] R. E. Cohen, *Nature (London)* **358**, 136 (1992).
 - [4] R. D. King-Smith and D. Vanderbilt, *Phys. Rev. B* **49**, 5828 (1994).
 - [5] A. von Hippel, R. G. Breckenridge, F. G. Chesley, L. Tisza, *Ind. Eng. Chem.* **38**, 1097 (1946).
 - [6] K. M. Rabe, *Antiferroelectricity in Oxides: A Reexamination* (Wiley-VCH, Verlag, 2013), pp. 221–244.
 - [7] T. Nishimatsu, M. Iwamoto, Y. Kawazoe, and U. V. Waghmare, *Phys. Rev. B* **82**, 134106 (2010).
 - [8] U. V. Waghmare and K. M. Rabe, *Phys. Rev. B* **55**, 6161 (1997).
 - [9] U. V. Waghmare, *Acc. Chem. Res.* **47**, 3242 (2014).
 - [10] W. Zhong, D. Vanderbilt, and K. M. Rabe, *Phys. Rev. B* **52**, 6301 (1995).
 - [11] D. J. Singh and L. L. Boyer, *Ferroelectrics* **136**, 95 (1992).
 - [12] W. Kohn and L. J. Sham, *Phys. Rev.* **140**, A1133 (1965).
 - [13] T. Hashimoto, T. Nishimatsu, H. Mizuseki, Y. Kawazoe, A. Sasaki, and Y. Ikeda, *Jpn. J. Appl. Phys.* **43**, 6785 (2004).
 - [14] D. I. Bilc, R. Orlando, R. Shaltaf, G.-M. Rignanese, J. Íñiguez, and P. Ghosez, *Phys. Rev. B* **77**, 165107 (2008).
 - [15] J. P. Perdew, K. Burke, and M. Ernzerhof, *Phys. Rev. Lett.* **77**, 3865 (1996).
 - [16] J. P. Perdew, K. Burke, and M. Ernzerhof, *Phys. Rev. Lett.* **80**, 891 (1998).
 - [17] Z. Wu and R. E. Cohen, *Phys. Rev. B* **73**, 235116 (2006).
 - [18] J. Sun, A. Ruzsinszky, and J. P. Perdew, *Phys. Rev. Lett.* **115**, 036402 (2015).
 - [19] J. Sun, R. C. Remsing, Y. Zhang, Z. Sun, A. Ruzsinszky, H. Peng, Z. Yang, A. Paul, U. Waghmare, X. Wu, M. L. Klein, and J. P. Perdew, *Nat. Chem.* **8**, 831 (2016).
 - [20] D. A. Kitchaev, H. Peng, Y. Liu, J. Sun, J. P. Perdew, and G. Ceder, *Phys. Rev. B* **93**, 045132 (2016).
 - [21] Z.-H. Yang, H. Peng, J. Sun, and J. P. Perdew, *Phys. Rev. B* **93**, 205205 (2016).
 - [22] G. Kresse and J. Furthmüller, *Phys. Rev. B* **54**, 11169 (1996).
 - [23] G. Kresse and J. Furthmüller, *Comput. Mater. Sci.* **6**, 15 (1996).
 - [24] G. Kresse and D. Joubert, *Phys. Rev. B* **59**, 1758 (1999).
 - [25] T. Nishimatsu, U. V. Waghmare, Y. Kawazoe, and D. Vanderbilt, *Phys. Rev. B* **78**, 104104 (2008).
 - [26] Computer code FERAM, <http://loto.sourceforge.net/feram/> (unpublished).
 - [27] S. D. Bond, B. J. Leimkuhler, and B. B. Laird, *J. Comput. Phys.* **151**, 114 (1999).
 - [28] A. I. Lebedev, *Phys. Status Solidi B* **249**, 789 (2012).
 - [29] G. H. Kwei, A. C. Lawson, S. J. L. Billinge, and S. W. Cheong, *J. Phys. Chem.* **97**, 2368 (1993).
 - [30] G. Shirane, H. Danner, A. Pavlovic, and R. Pepinsky, *Phys. Rev.* **93**, 672 (1954).

- [31] A. I. Frenkel, F. M. Wang, S. Kelly, R. Ingalls, D. Haskel, E. A. Stern, and Y. Yacoby, *Phys. Rev. B* **56**, 10869 (1997).
- [32] L. F. Wan, T. Nishimatsu, and S. P. Beckman, *J. Appl. Phys.* **111**, 104107(2012).
- [33] S. Piskunov, E. Heifets, R. Eglitis, and G. Borstel, *Comput. Mater. Sci.* **29**, 165 (2004).
- [34] R. O. Bell and G. Rupprecht, *Phys. Rev.* **129**, 90 (1963).
- [35] Z. Li, M. Grimsditch, C. Foster, and S.-K. Chan, *J. Phys. Chem. Solids* **57**, 1433 (1996).
- [36] I. Tomeno, Y. Tsunoda, K. Oka, M. Matsuura, and M. Nishi, *Phys. Rev. B* **80**, 104101 (2009).
- [37] K. Ueda, H. Yanagi, R. Noshiro, H. Hosono, and H. Kawazoe, *J. Phys.: Condens. Matter* **10**, 3669 (1998).
- [38] W. Zhou, H. Deng, P. F, and J. Chu, *Appl. Phys. Lett.* **105**, 111904 (2014).
- [39] G. Li, T. Kako, D. Wang, Z. Zou, and J. Ye, *J. Solid State Chem.* **180**, 2845 (2007).
- [40] S. Piskunov, A. Gopeyenko, E. Kotomin, Y. Zhukovskii, and D. Ellis, *Comput. Mater. Sci.* **41**, 195 (2007).
- [41] R. Eglitis, *Solid State Ionics* **230**, 43 (2013).
- [42] C.-Z. Wang, R. Yu, and H. Krakauer, *Phys. Rev. B* **54**, 11161 (1996).
- [43] R. Wahl, D. Vogtenhuber, and G. Kresse, *Phys. Rev. B* **78**, 104116 (2008).
- [44] O. Dieguez, K. M. Rabe, and D. Vanderbilt, *Phys. Rev. B* **72**, 144101 (2005).
- [45] K. M. Rabe and U. V. Waghmare, *Phys. Rev. B* **52**, 13236 (1995).
- [46] T. Nishimatsu, K. Aoyagi, T. Kiguchi, T. J. Konno, Y. Kawazoe, H. Funakubo, A. Kumar, and U. V. Waghmare, *J. Phys. Soc. Jpn.* **81**, 124702 (2012).
- [47] C. J. Johnson, *Appl. Phys. Lett.* **7**, 221 (1965).
- [48] H. Krakauer, R. Yu, C.-Z. Wang, K. M. Rabe, and U. V. Waghmare, *J. Phys.: Condens. Matter* **11**, 3779 (1999).
- [49] G. Shirane, R. Pepinsky, and B. C. Frazer, *Acta Crystallogr.* **9**, 131 (1956).
- [50] Computer code ISOTROPY software suite, <http://iso.byu.edu> (unpublished).